COMPUTATION OF AEOLIAN TONE NOISE FROM TWIN CYLINDERS BY USING GRID-OPTIMIZED DISPERSION-RELATION-PRESERVING SCHEMES WITH IMMERSED SURFACE DIPOLE MODEL

Cheolung Cheong[*], Jewook Ryu[#], and Soogab Lee[†]

School of Mechanical and Aerospace Engineering
Seoul National University
Seoul 151-742, Korea

ABSTRACT

Grid-Optimized Dispersion-Relation-Preserving (GODRP) schemes are used for the computation of category 5, problem 1 in 4th CAA Workshop. Tam's DRP scheme is implemented only on a uniform Cartesian grid while practical problems in aeroacoustics are seldom confined to uniform Cartesian geometry, with the associated computational grids usually being non-uniform or curvilinear. The GODRP schemes have been developed with grid-optimization algorithm to make finite difference equations possess the same dispersion relations as the corresponding partial differential equations on general geometries. Acoustic/viscous splitting techniques with immersed surface dipole model (ISDM) are utilized to solve the sound generation and propagation in viscous, low-Mach number flows for which direct computation of the aerodynamic noise remains difficult because of the large computing resources, the expensive cost and physical/numerical issues inherent in CAA. The ISDM is recently developed for the efficient computation of aerodynamic noise generation and propagation in low Mach number flows in which dipole source, originating from unsteady pressure fluctuation on a solid surface, is known to be more efficient than quadrupole sources. The multi-scale overset grid technique is also applied to resolve the complex geometries. Through the illustrative application to the benchmark problem, it will be shown that the current methods can broaden the application area of computational aeroacoustic techniques to practical aeroacoustic phenomena, enhancing both the speed and accuracy of the computation.

INTRODUCTION

Aeolian tones from flow over cylinders are relevant to airframe and power plant noise (tubular heat exchanger, power transmission lines and chimneys). The purpose of this benchmark problem is to test the ability of a CFD/CAA code to accurately and effectively predict sound generation by viscous flows over a blunt body and sound propagation through interactions with solid wall and moving flows.

Numerical dissipation and numerical dispersion are the two primary sources of error associated with computational schemes. Recent reviews of computational aeroacoustics by Tam (ref. 1) and Wells et al. (ref. 2) have discussed various numerical schemes currently popular in CAA. These include many compact and non-compact optimized schemes such as the family of high-order compact differencing schemes (refs. 3 to 5) and DRP scheme (ref. 6). They are all centered non-dissipative schemes, a property that is desirable for linear wave propagation. However, the DRP scheme has been more favored due to its simple and robust algorithm. The DRP scheme is implemented by using a symmetric finite difference stencil on a uniform Cartesian Grids. In this environment, the classic DRP schemes minimize numerical dispersion errors while producing essentially no dissipation errors. However, practical problems in aeroacoustics are seldom confined to uniform Cartesian geometry, with the associated computational grids usually being non-uniform or curvilinear. GODRP schemes (ref. 7) have been developed with the grid-optimization algorithm to make the finite difference equations possess the same dispersion relations as the corresponding partial differential equations and, at the same time, optimized dissipation characteristics at the given grids that are the non-uniform Cartesian or curvilinear grids. In this work, the GODRP schemes are utilized to solve this complex geometry problem with curvilinear grids on a guarantee of local and, thus resultant global dispersion-relation-preserving properties.

[*] BK21 Post Doctor, accu99@snu.ac.kr
[#] Ph. D. Candidate, jwryu1@snu.ac.kr
[†] Professor, solee@plaza.snu.ac.kr, Bldg. 301-1303, Seoul National University, Seoul 151-742, Korea

For many industrial problems originating from aerodynamic noise, computational aeroacoustics (CAA) technique, reliable and easy to apply, would be of great value to engineers and manufacturers. Recent and spectacular achievements in the understanding of aerodynamic noise generation mechanism are based on the CAA technique using the direct calculation of the acoustic field by solving the unsteady compressible Navier-Stokes equations. Most of them are related to jet noise phenomena, on which the direct numerical simulations (ref. 8) are carried out, providing directly an acoustic far field conformable to measurements. However, direct computation of the aerodynamic noise radiated by a subsonic flow remains difficult because of the large computing resources, the expensive cost and physical/numerical issues (ref. 1) inherent in CAA. These difficulties lead to alternative methods, so-called hybrid methods. These methods are based on the concept of variable decomposition in the governing equations into a source component and an acoustic one, which leads to two separate sets of equations governing viscous flow field and acoustic disturbance field, respectively. This approach is based on the assumption that the wave propagation is essentially inviscid in nature and sound perturbations are so small that their contribution to the convection velocity of the flow is negligible in most cases. The most important advantage of the decomposition method is that algorithms are used that best suited to each solver: traditional CFD algorithms for the viscous flow and CAA algorithms for the acoustic perturbations. These separate solvers accommodate the disparate length scales (i.e., acoustic and convective) associated with low Mach number aeroacoustics. The convective length scales are resolved on a hydrodynamic grid, while the acoustic length scales are resolved on a separate acoustic grid. Immersed surface dipole model (ISDM, ref. 9) are recently developed for the efficient computation of aerodynamic noise generation and propagation in low Mach number flows in which dipole source, originating from unsteady pressure fluctuation on a solid surface, is known to be more efficient than quadrupole sources. In this work, ISDM combined with the acoustic/viscous splitting method is utilized for this low-Mach number aeroacoustic problem.

It is very difficult to construct a single body-fitted mesh for twin cylinders which gives the proper resolution to both the near source region and far acoustic field. The complex geometries and large disparate length scales are overcome by the use of a multi-scale overset grid technique, where body-fitted meshes are applied only near the cylinders and multi-scale Cartesian background mesh is applied elsewhere.

In Section 2, fundamental formulations for the acoustic disturbance are given. The model of immersed surface dipole source terms forcing the disturbance equations is presented. Incompressible Navier-Stokes equations and turbulence model for viscous flow are also given. In Section 3, numerical methods for the acoustic and flow solvers are described. General numerical method modeling the surface dipole source terms is also given. In Section 4, Aeolian tone from the cross flow past twin-cylinders are investigated with the prescribed methods. Detailed discussion on the numerical results is presented. Final section is devoted to the concluding remarks.

FUNDAMENTAL EQUATIONS

The wave generation process is generally believed to be hardly affected by viscosity. We therefore begin with the unsteady Euler equations

$$\frac{\partial \rho}{\partial t}+\frac{\partial}{\partial x_j}\rho v_j = 0\,,\ \frac{\partial}{\partial t}\rho v_i+\frac{\partial}{\partial x_j}\rho v_i v_j+\frac{\partial p}{\partial x_i}=0 \ \text{ and } \frac{\partial}{\partial t}\rho e_0+\frac{\partial}{\partial x_j}\rho h_0 v_j = 0\cdot \tag{1}$$

where $e_0 \equiv e+1/2\cdot v^2$ denotes the stagnation total energy (e = total energy) and $h_0 \equiv h+1/2\cdot v^2$ represents the stagnation total enthalpy (h = the enthalpy). The energy conservation equation of (1) can be transformed to an equation for the pressure p by using the relation $(\partial e/\partial p)_s = p/\rho^2 c^2$.

$$\frac{\partial p}{\partial t}+v_j\frac{\partial p}{\partial x_j}+\gamma p\frac{\partial v_j}{\partial x_j}=0 \tag{2}$$

Where γ designates the ratio of specific heats, and is taken as $\gamma = 1.4$ for air. This equation (2) will be used instead of the energy equation because pressure is a quantity of great interest to acoustic problems.

The dependent variables can be divided into their base flow components and into their residual components such that $\rho=\overline{\rho}+\rho'$, $p=\overline{p}+p'$ and $v_i=\overline{v}_i+v_i'$. By inserting these decomposed variables to Eqs. (1) and (2) and then, by subtracting the resultant equations from the viscous flow equations satisfied by the base flow components, governing equations for the residual components can be obtained. It is evident that different choice of the base flow variables leads to the different forms of acoustic governing equations (ref. 10).

If the base flow is a steady mean flow, the 2-D governing equations for the residual components are written as the following form (ref. 11).

$$\frac{\partial \mathbf{U}}{\partial t}+\frac{\partial \mathbf{E}}{\partial x}+\frac{\partial \mathbf{F}}{\partial y}+\frac{\partial \mathbf{E}_{nl}}{\partial x}+\frac{\partial \mathbf{F}_{nl}}{\partial y}+\mathbf{H}=\mathbf{S} \tag{3}$$

where **U** is the unknown vector, **E** and **F** are the linear flux vectors, $\mathbf{E}_{nl}$ and $\mathbf{F}_{nl}$ are the nonlinear flux vectors, and the vector **H** consists of mean flow gradient terms, which are equal to zero when mean flow is uniform. The vector **S** represents possible unsteady sources in the flow.

Assuming isentropic flows, noise generation is provided by source terms in the momentum equation of Eq. (3). In present method, the source terms are modeled with the immersed surface dipoles (ref. 9) of magnitude corresponding to the hydrodynamic unsteady pressure fluctuations on a solid surface.
First, let's introduce a function f*(x,t)* where f is negative within the control surface, positive within the surrounding fluid and f also satisfies the equations $|\nabla \mathrm{f}| = 1$. Also, define a Heaviside function H*(x),* by

$$\mathrm{H}(x)=\begin{cases}1 & for \quad x>0\\ 0 & for \quad x<0\end{cases} . \tag{4}$$

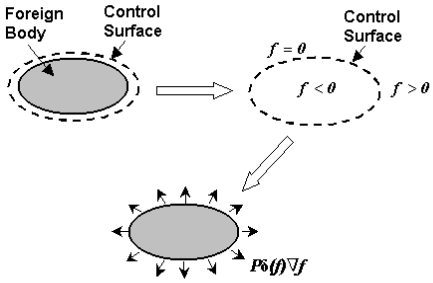

Figure 1. Schematic diagram of the procedure for the immersed surface dipole modeling

Then H(f) vanishes within the control surface and is equal to unity in the region exterior to the surface. Gradient of given fluctuating pressure in a solid body can be recast into the following form,

$$\nabla\left(P\cdot \mathrm{H(f)}\right)=\mathrm{H(f)}\nabla P+P\nabla \mathrm{H(f)}=\mathrm{H(f)}\nabla P+P\nabla \mathrm{f}\delta(\mathrm{f}) \tag{5}$$

where $P(\mathbf{x},t)=p(\mathbf{x},t)-p_0(\mathbf{x})$ and $p_0(\mathbf{x})=\lim_{T\to\infty}\frac{1}{T}\int_{-T}^{T}p(\mathbf{x},t)dt$

Then, in computation domain,

$$\nabla\left(P\cdot H(f)\right)=P\nabla f\delta(f) . \tag{6}$$

Then, the vector **S** is written as

$$\mathbf{S}=\begin{bmatrix}0 & S_1 & S_2 & 0\end{bmatrix}^T=\begin{bmatrix}0 & P\delta(\mathrm{f})\nabla \mathrm{f}_1 & P\delta(\mathrm{f})\nabla \mathrm{f}_2 & 0\end{bmatrix}^T \tag{7}$$

Data provided by incompressible or compressible simulations can be used to estimate S_i. The compressible simulations, however, must be used with special caution. In the compressible case, the acoustic field is included in the source terms, through density and fluctuating velocity. Although these acoustic components are very small compared to hydrodynamic fluctuations, they decay very slowly. Hence, their contribution might have a considerable influence on the predicted acoustic pressure magnitudes. The philosophy of covering a body surface with immersed surface dipole models (ISDM) is schematically described in Fig. 1.

Present approach is focused on low Mach number flows. Thus the 2-D incompressible Reynolds-Averaged Navier-Stokes (RANS) equations are used as the governing equations for viscous flow. Eddy viscosity ν_t is modeled from the low Reynolds number κ– ε turbulence model by Chen et al. (ref. 12).

NUMERICAL METHODS

The Cartesian coordinates employed in equation (3) are inconvenient for complex geometries. The spatial derivatives expressed as functions of coordinates (x, y) may be recast as functions of curvilinear coordinates (ξ, η) by a general transformation. Then, Eq. (3) in a physical domain is expressed by the coordinate variables in a computational domain.

$$\frac{\partial \mathbf{U}^*}{\partial t}+\frac{\partial \mathbf{E}^*}{\partial \xi}+\frac{\partial \mathbf{F}^*}{\partial \eta}+\frac{\partial \mathbf{E}^*{}_{nl}}{\partial \xi}+\frac{\partial \mathbf{F}^*{}_{nl}}{\partial \eta}+\mathbf{H}=\mathbf{S} \tag{8}$$

where $\mathbf{U}^* = \frac{\mathbf{U}}{J}$, $\mathbf{E}^* = \frac{1}{J}\left(\xi_x \mathbf{E} + \xi_y \mathbf{F}\right)$, $\mathbf{F}^* = \frac{1}{J}\left(\eta_x \mathbf{E} + \eta_y \mathbf{F}\right)$, $\mathbf{E}^*_{nl} = \frac{1}{J}\left(\xi_x \mathbf{E}_{nl} + \xi_y \mathbf{F}_{nl}\right)$, and $\mathbf{F}^*_{nl} = \frac{1}{J}\left(\eta_x \mathbf{E}_{nl} + \eta_y \mathbf{F}_{nl}\right)$.

Here, $J = \left(x_\xi y_\eta - x_\eta y_\xi\right)^{-1}$.

All the variables are nondimensionalized with the following scales: D (diameter of a cylinder) for the length scale, c_∞ for the velocity scale, D/c_∞ for the time scale, ρ_∞ for the density scale and $\rho_\infty c_\infty^2$ for the pressure scale, where c_∞ is the ambient speed of sound. The 7-point stencil, Grid-Optimized Dispersion-Relation-Preserving (GODRP) Scheme of Cheong & Lee (ref. 7) is utilized for the spatial flux derivatives of Eq. (8). Tam & Webb (ref. 6) have shown that if a given numerical scheme and the governing equations have the same dispersion relations, the numerical and exact solutions will have the same wave propagation characteristics and wave speeds. The GODRP schemes have been developed with the grid-optimization algorithm to make the finite difference equations possess the same dispersion relations as the corresponding partial differential equations on general geometries. Eq. (8) is discretized in space by the GODRP scheme as

$$\frac{\partial \mathbf{U}_{i,j}}{\partial t} = -\sum_{l=-3}^{l=3}\left[a_{\xi l\quad (i,j)}\left(\mathbf{E}^*_{i+l,j} + \mathbf{E}^*_{nli+l,j}\right) + a_{\eta l\quad (i,j)}\left(\mathbf{F}^*_{i,j+l} + \mathbf{F}^*_{nli,j+l}\right)\right] - \mathbf{H}_{i,j} + \mathbf{S}_{i,j} \tag{9}$$

where $a_{\xi l(i,j)}$ and $a_{\eta l(i,j)}$ are the l^{th} optimized coefficients of the GODRP finite difference scheme at the (i, j) points along the ξ- and η- direction, respectively. The coefficients is chosen by requiring that the numerical wave number vectors of the finite difference scheme be a close approximation to the exact wave number of the corresponding partial differential equations. For more detailed description on the GODRP scheme, refer to ref. 7. In some cases it is necessary to remove spurious numerical oscillations due to non-linearities or mismatches with the boundary conditions or the initial conditions. These short waves can be filtered by an artificial selective damping proposed by Tam & Shen (ref. 13). Time integration is performed with the low-dissipation and low-dispersion Runge-Kutta schemes by Hu et al. (ref. 14) for their minimized dissipation and dispersion errors for wave propagation. Across the outflow boundaries of the computational domain, flow of information is associated with acoustic waves, vorticity waves and entropy waves. At these boundaries there is only one incoming characteristic, and only the pressure perturbation satisfies the convected wave equation. Therefore, B_1 operator of Bayliss and Turkel (ref. 15) is also used here, but for the pressure perturbation only. The other boundary conditions are formed by the linearized momentum equations and the equation of conservation of the acoustic speed, as adapted from Tam and Webb (ref. 6). For a high-order finite difference scheme the order of the difference equations is higher than that of the Euler equations. Thus the zero normal velocity boundary condition is insufficient for defining a unique solution. Extraneous numerical conditions must be imposed. Ghost value of pressure (ref. 16) is used as the extraneous boundary condition.

The very act of discretization causes many numerical artifacts. Modeling of the delta function in the analytic expression for immersed surface dipole sources is required for a discrete numerical simulation. The delta function is modeled as

$$\delta(\mathbf{x}) \cong \left(\ln 2/\pi\sigma^2\right)^{\frac{n}{2}} \exp(-\ln 2 \cdot \mathbf{x}^2/\sigma^2)\,, \tag{10}$$

where n (= *1* or *2* or *3*) denotes the dimension of delta function. Both sides of the equations satisfy the following space integral equation if $n = 2$.

$$\int_{-\infty}^{\infty}\int_{-\infty}^{\infty} \delta(\mathbf{x})dx_1dx_2 = \int_{-\infty}^{\infty}\int_{-\infty}^{\infty} \left(\ln 2/\pi\sigma^2\right)\exp(-\ln 2 \cdot \mathbf{x}^2/\sigma^2)dx_1dx_2 = 1 \tag{11}$$

Although Eq. (11) guarantees the conservation of total energy of the delta function, i.e., the acoustic sources, there is still difference in the distribution of source. It is evident that, as the value of σ is decreased, modeling Eq. (10) becomes more close approximation for the delta function. Combining (7) and (10), immersed surface dipole model is numerically expressed as

$$S_i(\mathbf{x},t) = P(\mathbf{x},t)\cdot\left(\ln 2/\pi\sigma^2\right)\exp(-\ln 2 \cdot \mathrm{f}(\mathbf{x},t)^2/\sigma^2)\nabla \mathrm{f}_i(\mathbf{x},t) \tag{12}$$

In real applications where a solid body exists, Eq. (12) needs to be slightly changed because the solid body replaces the some portion of the immersed surface dipole sources and thus, Eq. (11) can not be satisfied in a fluid region. Therefore, correction factor, C is multiplied to Eq. (12) as follows

$$S_i(\mathbf{x},t) = P(\mathbf{x},t)\cdot C\cdot\left(\ln 2/\pi\sigma^2\right)\exp(-\ln 2\cdot \mathrm{f}(\mathbf{x},t)^2/\sigma^2)\nabla \mathrm{f}_i(\mathbf{x},t) \tag{13}$$

where $C = 1\Big/\left(\int_{-\infty}^{\infty}\int_{-\infty}^{\infty}\left(\ln 2/\pi\sigma^2\right)\exp(-\ln 2\cdot\mathbf{x}^2/\sigma^2)dx_1dx_2 - \int_B\left(\ln 2/\pi\sigma^2\right)\exp(-\ln 2\cdot\mathbf{x}^2/\sigma^2)dx_1dx_2\right)$ and B denotes the region that the solid body occupies.

The numerical method used for viscous flow simulation is based on the unstructured grid finite volume method, which has been described in detail by Kang et al. (ref. 17). The scheme has extended the unstructured grid Navier-Stokes procedure for incompressible flows developed by Thomadakis et al. (ref. 18) to allow collocated storage of all variables. Since Thomadakis et al. used a staggered-grid formulation, pressure is stored at the centroid of a cell while velocity components are stored at grid points. However, the scheme has modified this procedure to employ collocated storage (non-staggered) in order to obviate the difficulties and disadvantages of implementing a non-collocated (staggered) mesh within the unstructured methodology. The algebraic pressure equation is derived by substituting the discretized momentum equations into the continuity equation (ref. 19). The process of deriving the pressure equation is almost the same as one used for a structured grid method. The scheme uses the Quadratic Upstream Interpolation for Convective Kinematics (QUICK) scheme for the convective terms and the second order Euler backward difference for time derivatives to keep second order accuracy spatially and temporally. All other spatial derivatives are approximated by the central difference schemes.

NUMERICAL RESULTS

1. Numerical Results for Viscous Flow Simulations

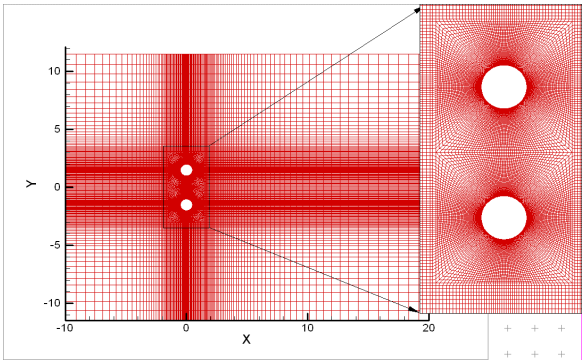

Figure 2. The mesh for the viscous flow simulation

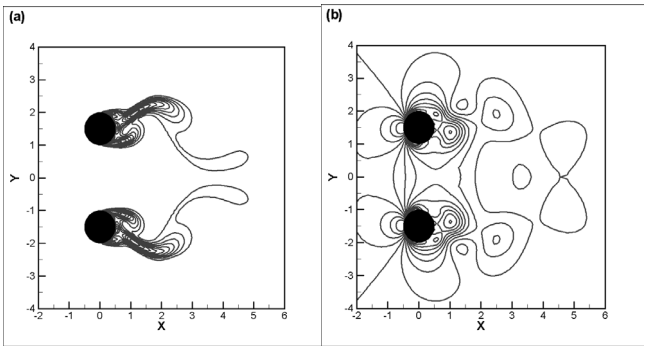

Figure 3. Instantaneous, non-dimensional (a) *k, 10 levels from 0.1 to 1.0* and (b) Pressure contours, 13 levels from –0.8 to 0.4

The flow calculations are carried out on a mesh with approximately 41,103 points in the computational domain. Pictures of the mesh and its close-up are shown in Fig.2. The mesh for viscous flow simulation consists of two types of grids: Inner mesh is the multiply connected grid and outer one is the Cartesian grid. Initially, random disturbances are imposed on a uniform velocity to quickly generate vortex shedding. The computational time step is fixed to be $\Delta t = 0.01/(D/u_\infty)$. Fig. 3 shows the iso-contours of turbulence kinetic energy and pressure at certain time instant. It is evident that Anti-phase lift and In-phase drag forces exerted on the cylinder surface fluctuate in time due to the periodic shedding of vortices. The frequency or period of vortex shedding can be estimated by evaluating those of the oscillating lift or drag coefficient. Time-dependent signals of lift and drag coefficients are presented in Fig. 4, where the lift and drag coefficients. As the computation

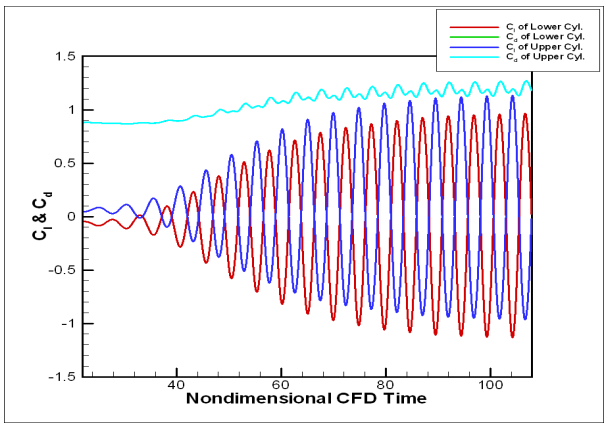

Figure 4. Time dependent signals of C_l and C_d

begins with an initial condition that is given by the flow solutions, vortex shedding does not occur for a considerable time. However, after the first shedding happens, the flow goes through a transient state to arrive to the state of periodic shedding of vortices. Lift and drag coefficients show a sinusoidal variation corresponding to a Strouhal number of 0.2 and 0.4, respectively. This value is in good agreement with the experimental measurement (ref. 20).

2. Numerical Results of CAA Solver

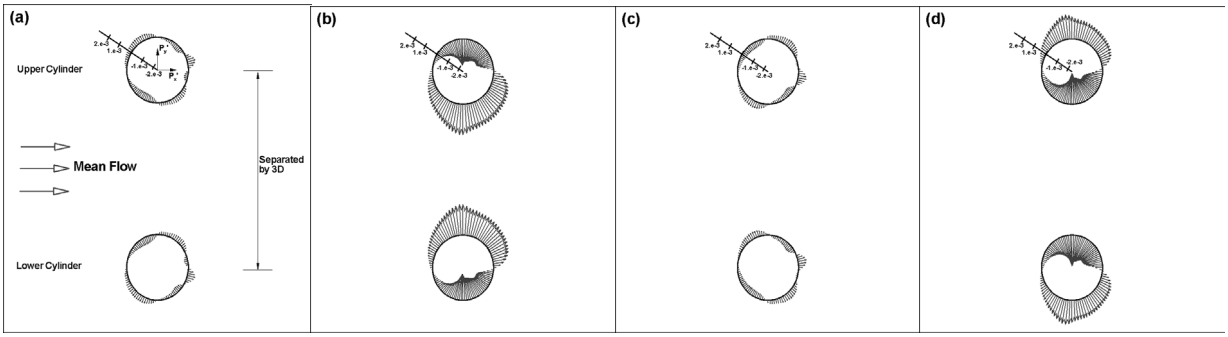

Figure 5. A sequence of simultaneous surface fluctuating pressure ($P = p - p_0$) at (a) one quarter of a cycle, (b) a half cycle, (c) three quarters of a cycle, (d) the beginning of a cycle.

Hydrodynamic unsteady data provided by the previously calculated viscous flow simulation using incompressible RANS are now used to build up the source terms of Eq. (7). They are recorded every iteration during one period on solid surfaces for dipole sources. Non-dimensional period T_f of the flow simulation equals 4.*9* with $\Delta t_f = 0.01$, i.e. 490 data points. Unsteady hydrodynamic pressures corresponding to dipole sources are stored on the cylinder surfaces consisting of 101 grid points, respectively. Physical time is non-dimensionalized by D/U_∞ in the viscous flow simulation and by D/C_∞ in the acoustic simulation. Different time-scale of the acoustic simulation from the viscous flow simulation

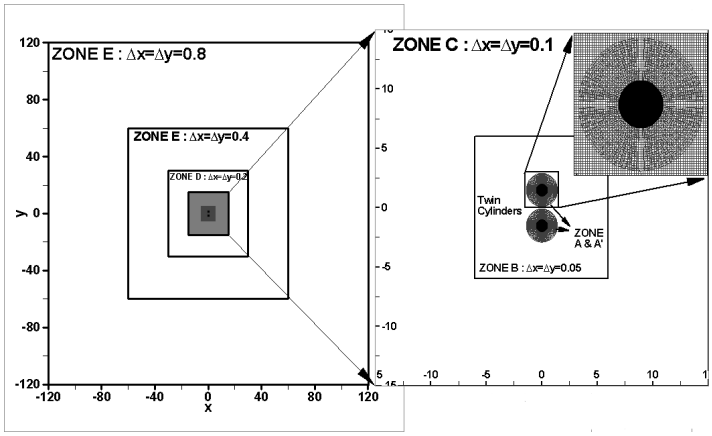

Figure 6. Multi-scale overset grid for the acoustic simulation

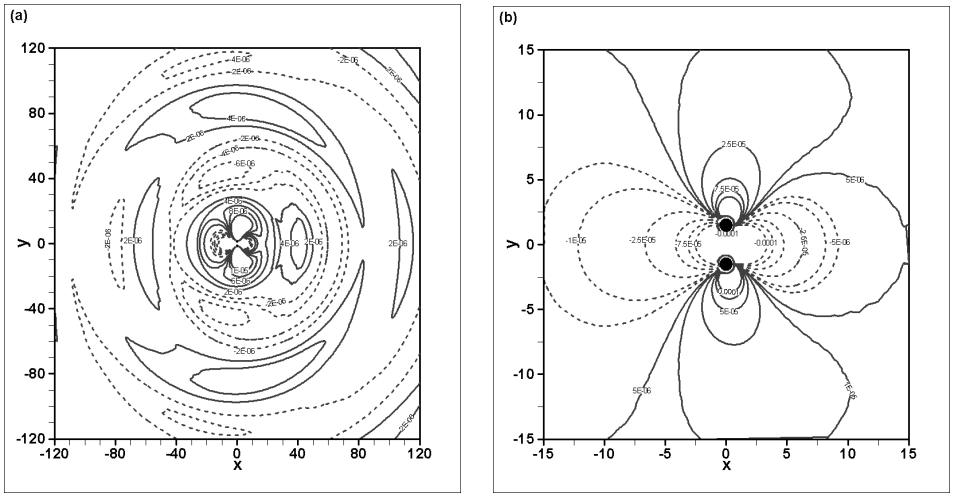

Figure 7. Instantaneous fluctuating pressure distribution at T = 180 (a) over whole field and (b) at near field

leads to the different non-dimension period $T_a = 68.08$ and numerical time step $\Delta t_a = 0.02$, i.e. *3404* data points. Furthermore, full computation domain of the computational aeroacoustics covers the far-field reaching to *120D* in this computation, i.e. acoustic field as well as the near-field, i.e. source field. Thus raw data of the viscous flow are transformed into those of the acoustic grid and time by interpolation in space and time. Figures 5 shows the fluctuating pressure *P* on the cylinder surface at one quarter of a cycle, at a half cycle, at three quarters of a cycle and at the beginning of a cycle, respectively. It is also observed that the fluctuating pressures show symmetric patterns. Fluctuating pressure data are utilized as input data to the immersed surface dipole model. The acoustic calculations are performed on a multi-scale overset mesh where body-fitted meshes are applied only near the cylinders and multi-scale Cartesian background meshes are applied elsewhere in the domains (see Fig. 6). Interpolation algorithm of Bin et al. (ref. 21) is used for the information exchange between the meshes. In this paper, acoustic calculations are executed without mean flow, i.e. with only the modeled source terms because of the shortage of the allowed paper length. .

In Fig. 7, fluctuating pressure field obtained from the simulation using the ISDM in ambient condition is plotted at non-dimensional time $T = 180$. As expected, the acoustic waves from lift and drag dipoles are mainly propagated in the direction normal and parallel to the mean velocity, respectively. Fig. 8 shows the pressure waveform along the y-axis ($y < 0$) at various times. These waveforms conform to the 2-dimensional wave propagation characteristics, i.e. decaying proportional to $r^{-0.5}$. The directivity patterns of the current simulation using the ISDM without mean flow, measured at $r = 10D$ *and* $r = 100D$ are shown in Fig. 9. The amplitudes of the fluctuating pressures from the lift and drag dipole sources are comparable for each other at $r = 10D$ while acoustic waves from the lift dipoles are more strength that those from the drag dipoles at $r = 100D$. Nevertheless, due to anti-phase of the lift dipoles of twin cylinders, the amplitude of acoustic wave in the direction normal to the mean-flow is reduced compared with that from single cylinder.

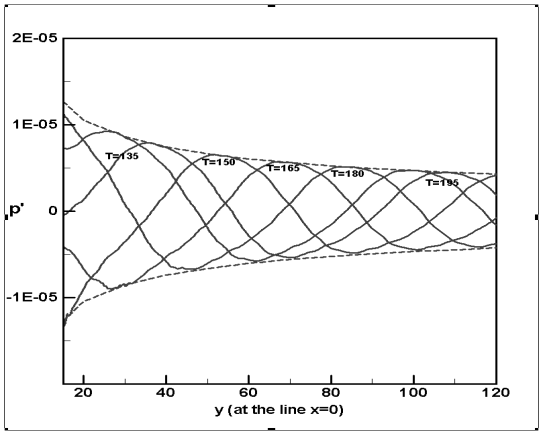

Figure 8. pressure distribution along the y-axis : —— numerical results, – – – decay lines correspond to $a/r^{0.5}$ where *a* is the value of pressure at $y = 100$ in the lines of $T = 135$.

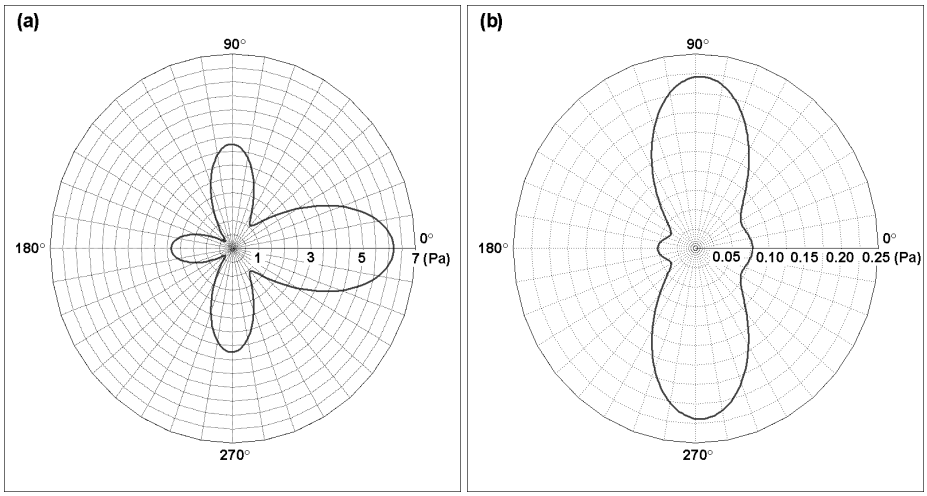

Figure 9. Directivity patterns of the mean square value of the fluctuating pressure (a)at $r = 10D$ and (b) at $r = 100D$

CONCLUDING REMARKS

The Grid-Optimized Dispersion-Relation-Preserving (GODRP) schemes are used for the computation of category 5, problem 1 in 4th CAA Workshop. The GODRP schemes have been developed with the grid-optimization algorithm to make the finite difference equations possess the same dispersion relations as the corresponding partial differential equations on general geometries. Acoustic/viscous splitting techniques with immersed surface dipole

model (ISDM) are utilized to solve the sound generation and propagation in viscous, low-Mach number flows for which direct computation of the aerodynamic noise remains difficult because of the large computing resources, the expensive cost and physical/numerical issues inherent in CAA. ISDM is recently developed for the efficient computation of aerodynamic noise generation and propagation in low Mach number flows in which dipole source, originating from unsteady pressure fluctuation on a solid surface, is known to be more efficient than quadrupole sources. The multi-scale overset grids technique is also applied to resolve the complex geometries. Through the illustrative application to the benchmark problem, it is shown that the current methods can broaden the application area of computational aeroacoustic techniques to practical aeroacoustic phenomena, enhancing both the speed and accuracy of the computation.

REFERENCES

1. Tam, C. K. W.: Computational Aeroacoustics: Issues and Methods. *AIAA J.* **33**,1995, pp. 1788-1796.
2. Wells, V.L.; and Renaut, R.A.: Computing Aerodynamically Generated Noise. *Annual Review of Fluid Mechanics* **29**, 1997, pp. 161-199.
3. Kim, J.W.; and Lee, D. J.: Optimized Compact Finite Difference Schemes with Maximum Resolution. *AIAA J.* **34**, 1996, pp. 887-893.
4. Deng, X.; and Zhang, H.: Developing High-order Weighted Compact Nonlinear Schemes. *J. Comput. Phys.* **165**, 2000, pp. 1-23.
5. Lele, S.K.: Compact Finite Difference Schemes with Spectral-Like Resolution. *J. Comput. Phys.* **103**, 1992. pp. 16-42.
6. Tam, C.K.W.; and Webb, J.C.: Dispersion-Relation-Preserving Schemes for Computational Acoustics. *J. Comput. Phys.* **107**, 1993, pp. 262-281.
7. Cheong, C.; and Lee, S.: Grid-optimized dispersion-relation-preserving schemes on general geometries for computational aeroacoustics. *J. Comput. Phys.* **174**, 2001, 248-276.
8. Freund, J. B.: Acoustic Sources in a Turbulent Jet: A Direct Numerical Simulation Study. Journal of Fluid Mechanics **438,** 2001, 277-305.
9. Ryu, J.; Cheong, C.; and Lee, S.: Efficient Computation of Flow Noise Generation and Propagation Using Immersed Surface Dipole Model Combined with Hybrid Methods. Journal of Sound and Vibration (In print)
10. Goldstein, M.E.; A unified approach to some recent developments in jet noise theory. International Journal of aeroacoustics **1**, 2002, pp.1-16.
11. Bogey, C.; Bailly, C.; and Juve D.: Computation of flow noise using source terms in linearized Euler's equations. AIAA J., 40, 2002, pp. 235-243.
12. Chen, K. Y.: Prediction of Channel and Boundary Layer Flows with a Low Reynolds Number Turbulence Model. *AIAA J.* 20, 1982, pp. 33-38,
13. Tam, C.K.W.; and Shen, H.: Direct computation on nonlinear acoustic pulses using high-order finite difference schemes. AIAA paper 93-4325, 1993.
14. Hu, F.Q.; Hussaini, M.Y.; and Manthey, J.L.: Low-dissipation and low-dispersion Runge-Kutta schemes for computational aeroacoustics. *J. Comput. Phys.* **124**, 1996, pp. 177-191.
15. Bayliss, A.; and Turkel, E.: Far field boundary conditions for compressible flow. *J. Comput. Phys.* **48**, 1982, pp. 182-199.
16. Tam, C.K.W.; and Dong, Z.: Wall boundary conditions for high-order finite difference schemes for computational aeroacoustics. *Theor. Comput. Fluid Dyn.* **8,** 1994, pp. 303-322.
17. Kang, D.J.; Bae, S.S.; and Joo, S.W.: An Unstructured FVM for the Numerical Prediction of Incompressible Viscous Flows. *Transactions of the KSME* **22,** 1998, pp. 1410-1421.
18. Thomadakis, M.; and Leschziner, M. A.: Pressure Correction Method for the Solution of Incompressible Viscous Flows on Unstructured Grids. *Int. J. Nume. Method in Fluids* **22**, 1996, pp. 581-600.
19. Hobson, G. V.; and Lakshiminarayana, B.: Prediction of Cascade Performance Using an Incompressible Navier-Stokes Technique. *J. Turbomachinery* **113**, 1991, pp. 561-572.
20. Kiya, M., et al.: Vortex Shedding From Two Circular Cylinders in Staggered Arrangement. Transactions of the ASME **102**, 1980, pp. 166-173.
21. Bin, J.; Cheong, C.; and Lee, S.; Optimized Boundary Treatment for Curved Walls for High-order Computational Aeroacoustics Schemes, *AIAA J.* (In print)